Eur. Phys. J. D (2017) 71: 231
DOI: 10.1140/epjd/e2017-80228-1

THE EUROPEAN PHYSICAL JOURNAL D

Regular Article

Energy partitioning and electron momentum distributions in intense laser-solid interactions*

Joel Magnusson[1,a], Arkady Gonoskov[1,2,3], and Mattias Marklund[1]

[1] Department of Physics, Chalmers University of Technology, 41296 Gothenburg, Sweden
[2] Institute of Applied Physics, Russian Academy of Sciences, 603950 Nizhny Novgorod, Russia
[3] Lobachevsky State University of Nizhni Novgorod, 603950 Nizhny Novgorod, Russia

Received 31 March 2017 / Received in final form 20 June 2017
Published online 7 September 2017

Abstract. Producing inward orientated streams of energetic electrons by intense laser pulses acting on solid targets is the most robust and accessible way of transferring the laser energy to particles, which underlies numerous applications, ranging from TNSA to laboratory astrophysics. Structures with the scale of the laser wavelength can significantly enhance energy absorption, which has been in the center of attention in recent studies. In this article, we demonstrate and assess the effect of the structures for widening the angular distribution of generated energetic electrons. We analyse the results of PIC simulations and reveal several aspects that can be important for the related applications.

1 Introduction

The interaction between high-intensity laser pulses and solids has been in the focus of researchers for a long period of time. Apart from being an experimental testbed for basic plasma phenomena, these interactions have several important applications, such as high harmonic generation (HHG) [1] or ion acceleration [2–4]. The latter has been widely studied due to the vast range of possible applications, e.g., biological or medical utilisations, of a table-top high-energy ion source. The overwhelming part of such studies relies on the target normal sheath acceleration (TNSA) scheme, in which the target's electrons are heated by the laser and then travel through the target to the rear side, where they create an electrostatic acceleration field for the ions [5–8]. There are many other schemes designed for ion acceleration (albeit exploiting different mechanisms), such as Coulomb explosion of clusters [9–11], double-layered targets [12–14], collisionless schock acceleration [15,16], hole boring [17], light sail acceleration (or laser piston acceleration) [18–21], and chirped standing wave acceleration [22].

The general simplicity of the TNSA mechanism and its robustness has made it easily accessible for experiments which by extension explains its popularity. Considerable effort has been put into the study of TNSA in order to fully understand and improve upon the basic scheme. Various studies have recently been performed of specially designed targets and laser pulse shapes [23–35].

However, it is well known that the TNSA scheme has several shortcomings, such as intrinsic angular and energy spread of the accelerated ions. Many of these shortcomings can be "engineered" away, i.e., by using a modified setup we can remedy, e.g., the angular spread. There are however basic restrictions that cannot be removed that easily. Most notably, the energy source is the laser pulse, and there is of course a limit on how much energy one can transfer from the laser to the target (and, therefore, to the ions). Theoretical and experimental studies show that the energy absorption can be significantly increased by structures on the surface [32,36–41], and the absorption can potentially be close to 100% [42,43]. As a natural continuation of these studies, we consider here how the structures affect the partitioning of the absorbed energy between the low and high energy electrons as well as between their normal and transverse motion. Apart from enhancing TNSA, the obtained results can be useful for developing alternative ion acceleration schemes that utilize transverse streams of electrons [25], as well as for other applications such as creating streams of electrons for laboratory astrophysics experiments.

2 Methods

In most attempts to improve our understanding of the TNSA scheme, the total absorbed laser energy and the

* Contribution to the Topical Issue "Relativistic Laser Plasma Interactions", edited by Tünde Fülöp, Francesco Pegoraro, Vladimir Tikhonchuk.

[a] e-mail: joel.magnusson@chalmers.se

resulting ion (typically protons) spectrum are considered. Analysing the total absorbed energy provides information about the initial stage of the process, of the interaction between the laser pulse and the plasma surface, while the ion spectrum essentially provides us with information integrated over the entire process. As important as these two sources of information are, this however does not provide us with the full picture. A large portion of the energy absorbed by the plasma at the front surface of the target can be "lost" instead of being transferred to the ions of interest: some hot electrons are transported away in the transverse directions, with some not even reaching the rear surface; electrons are backreflected and only transfer a small amount of their energy; and the transverse momentum of the hot electrons will not contribute to acceleration of the ions. A part of the laser energy can also be transformed into the energy of plasma surface waves [44,45]. In this paper we study the overall energy losses of these types. For this purpose we use PIC simulations that allow for all the outlined energy channels. However, in our analysis we differentiate only between three energy channels. For the transmitted electrons we consider the energy of longitudinal and transverse motion and the third channel is simply the energy not transferred through the plasma (i.e. the energy of reflected radiation and the energy of surface waves).

While the diagnostic tools available for experiments remain limited, thus making experimental studies of the intermediary stages of the TNSA process difficult, modern computational codes with the ability to act as new diagnostic tools can be used in order to bridge the gap and provide new insights into this intermediate regime. Here we will make use of the particle-in-cell (PIC) code PICADOR [46,47].

In order to study the effect of microstructured targets on the unwanted transverse transport of hot electrons and to be able to put this in relation to, for example, the absorbed energy, we need a measure of the energy related to motion in the forward (normal) and transverse directions. We define these quantities given the set of criteria that they should (1) be proportional to the kinetic energy of the electrons; (2) reflect upon the direction of the electrons; and (3) be additive. The final criterion is important as we want to ensure that addition of the transverse and forward energies yields the total kinetic energy of the electrons accounted for. Thus, we will use the definitions

$$\mathscr{E}_x = \sum_{\text{electrons}} \frac{p_x^2}{p_x^2 + p_y^2} m_e c^2 (\gamma - 1), \tag{1}$$

$$\mathscr{E}_y = \sum_{\text{electrons}} \frac{p_y^2}{p_x^2 + p_y^2} m_e c^2 (\gamma - 1), \tag{2}$$

$$\mathscr{E} = \mathscr{E}_x + \mathscr{E}_y = \sum_{\text{electrons}} m_e c^2 (\gamma - 1) = E_{\text{kinetic}}, \tag{3}$$

where m_e is the electron mass, c the speed of light, γ the Lorentz factor and p_x and p_y are the electron momenta in the x- and y-direction, respectively.

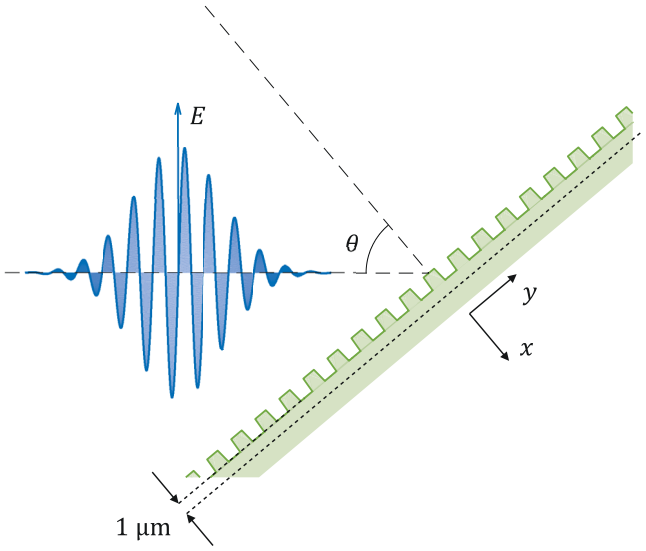

Fig. 1. The setup consists of a p-polarised Gaussian laser pulse incident on a microstructured, semi-infinite and overdense plasma at an angle to the target normal of θ. A virtual surface (dashed line), at which hot electron distributions are collected, is placed inside the plasma at a distance of 1 μm from the surface, not counting the height of the microstructures.

The quantities defined in equations (1)–(3) are then calculated for all electrons passing through a virtual surface placed inside the plasma at a distance of 1 μm from the plasma-vacuum boundary, as shown in Figure 1, and as we are only interested in the energy of the electrons travelling in the forward direction, we only account for electrons transiting this virtual surface in the positive x-direction ($p_x > 0$). Furthermore, we also track the total energy contained in as well as the energy entering and leaving the simulation region, providing us with exact knowledge of where the laser energy ends up.

2.1 Targets

The general setup of this study, presented in Figure 1, consists of a semi-infinite and overdense plasma with microstructures placed on the plasma-vacuum boundary. The virtual surface for counting transmitted particles is placed inside the plasma as previously discussed. The targets are then irradiated at an angle θ to the target normal by a p-polarised Gaussian laser pulse.

We study three different periodic microstructured designs, squares, triangles and circles (see Fig. 2). Each structure consists of a base shape of size $d \times d$, where we define d as the linear scale of the structure. This structure is then periodically repeated across an otherwise flat surface, with a periodicity of $2d$. While the density and composition of such structures are in general independent of the rest of the target, they will for the purpose of this paper be identical to the rest of the target. A flat target will also be studied as a reference.

When studying structures of varying sizes we will limit ourselves to sizes in the range $[\lambda/8,\ 4\lambda]$ in order

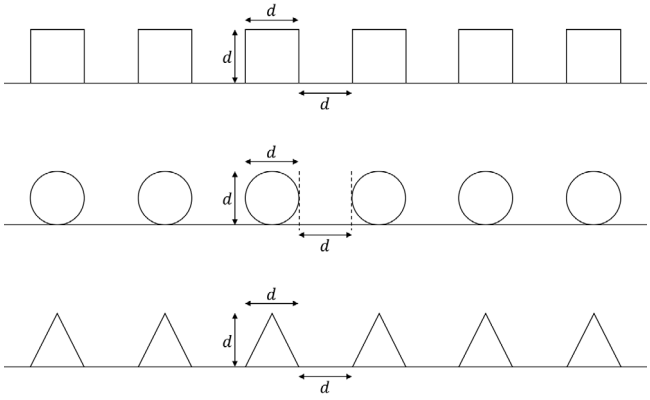

Fig. 2. The 2D geometry of the microstructured targets considered are completely described by a single scaling parameter, d, defining the maximum width and height as well as the minimal distance between the structures.

to ensure that (1) the structures are sufficiently resolved by the space step (space step $\ll d$) and (2) the effects due to alignment remains negligible ($d < w_0$). Moreover the density profile of the targets studied will be sharp, meaning a negligible preplasma. This allows us to study a cleaner setup and to clearly find cause-and-effects in the setups. Adding a preplasma to these microstructured targets would certainly be of interest, but is outside the scope of the current study.

2.2 Laser pulse

As we aim to use relevant laser parameters, available at most high-power laser facilities, we here consider a laser pulse of wavelength $\lambda = 810$ nm and energy $E = 1$ J, with a Gaussian profile focused to a FWHM beam waist radius $w_0 = 5$ μm. Its peak amplitude is consequently given by $a_0 = 6.3$ with a corresponding peak intensity of $I = 0.84 \times 10^{20}$ W/cm^2. The laser pulse is p-polarized in order to maximize the electron heating.

The targets are modeled to be of solid density with a number density of $n_0 = 30n_{cr}$, with critical density $n_{cr} = m_e\omega_0^2/4\pi e^2$ and where ω_0 is the laser pulse carrier frequency and e is the electron charge.

2.3 Numerical setup

In order to study the aforementioned target designs we have performed two-dimensional simulations using the PIC code Picador [46,47]. We resort to two dimensional simulations in order to keep the computational cost at a feasible level, however, this restriction is not likely to significantly affect our result as (1) the individual target geometries are two dimensional, (2) the interaction between the pulse and the plasma and the subsequent motion of the electrons are sufficiently described in the plane of incidence, and (3) two dimensions are sufficient for allowing important instabilities to form.

The targets are modeled as singly ionized plasmas consisting of electrons and heavy ions with mass $10m_p$ and charge $-e$, where m_p is the proton mass.

3 Results

When a flat foil is irradiated by a laser pulse at an angle θ, the strong localized heating of the plasma will generate highly energetic electrons. The momentum distribution of these hot electrons can be calculated for highly idealized setups. As the physics remain unchanged under Lorentz transformations we may instead consider the completely equivalent system of a laser pulse irradiating a flat foil of streaming plasma at normal incidence, which can then be treated as one-dimensional (see Fig. 3).

We now consider the problem in the boosted reference frame which moves with speed $v = c\sin\theta$ along the surface, in the y-direction. In this reference frame, prior to the interaction the momentum of an electron is given by

$$p'_y = -\gamma v/c = -\tan\theta, \tag{4}$$

where γ is the Lorentz factor and the momentum is given in units of $m_e c$.

Moreover, by consideration of conservation of generalized momentum we have that

$$p'_y + A'_y = \text{const}, \tag{5}$$

where A'_y is the vector potential as seen in the boosted frame, written in units where the absolute value of the electron charge is one. As the vector potential is zero both prior to and following the interaction, equation (5) implies that equation (4) holds also after the electron's interaction with the laser field.

Thus, by applying a boost v in the negative y-direction, we obtain the following expression for the electron's momentum in the lab frame and after the interaction

$$p_y = \frac{\sin\theta}{\cos^2\theta}\left(\sqrt{1 + p_x^2\cos^2\theta} - 1\right). \tag{6}$$

In two and three spatial dimensions, instabilities forming at the interaction surface will distort this and the collimation of the hot electrons will subsequently be decreased compared to the one dimensional case. This behaviour is easily recognizable in Figures 4a and 4b where the momentum space distribution of the generated hot electrons closely follows the predicted shape at the earlier stages of the interactions. The distribution follows this general trend all throughout the interaction, however when integrating over the entire process it can be clearly seen that it gets spread out, as expected.

The introduction of microstructures to the surface can drastically change this behaviour. The introduction of the structures increases the number of incidence angles experienced by the pulse as it interacts with the surface and further breaks the homogeneity present in the transverse direction of flat targets. As a result the hot electrons will be generated with a much broader momentum space

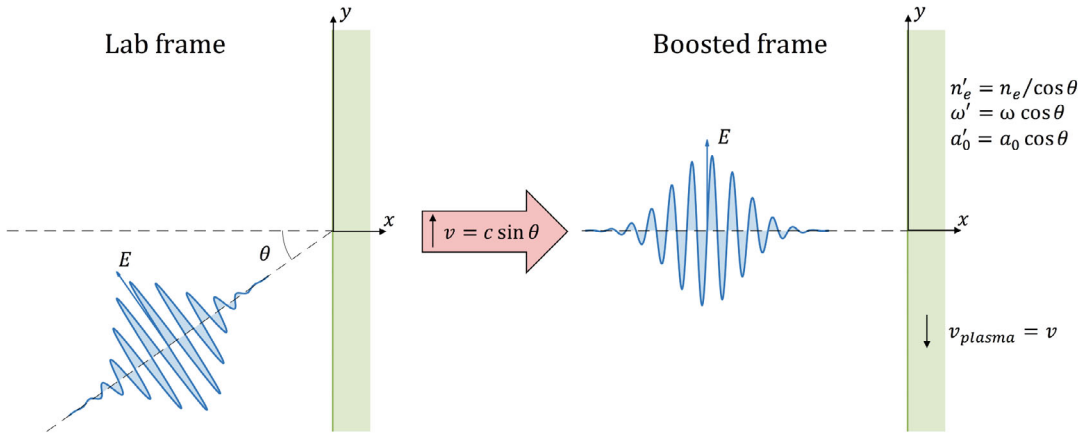

Fig. 3. A p-polarised laser pulse is incident on a flat plasma slab at an angle θ. A Lorentz boost of $v = c\sin\theta$ in the y-direction, along the surface in the plane of incidence, results in a boosted frame where the laser pulse is instead incident normally on a slab of plasma streaming in the negative y-direction with velocity v. The electron plasma density, pulse carrier wavelength and pulse amplitude will be transformed according to the shown relations, where the primed quantities are that of the boosted frame and where we have retained the units of the lab frame.

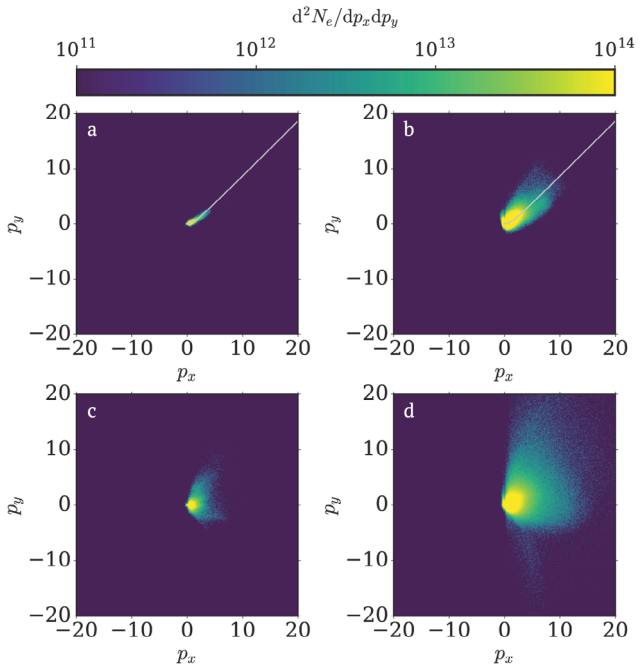

Fig. 4. The cumulative momentum space distribution of electrons transiting the virtual surface placed 1 μm inside the plasma for a flat foil (a, b) and a foil with $d/\lambda = 1/2$ square microstructures (c, d) when irradiated by a laser pulse incident at 45°. The momentum relation predicted by conservation of generalized momenta for an idealized flat foil is indicated with a light-gray line (a, b). The distribution is shown at $t = 225$ fs (a, c) and $t = 500$ fs (b, d).

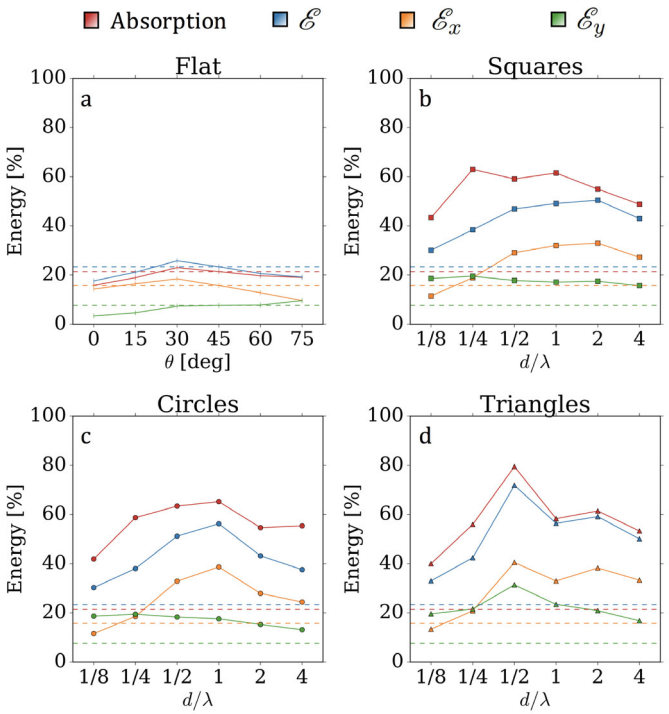

Fig. 5. The absorbed energy and the energy stored in forward and transverse motion of electrons when irradiating a flat foil at different angles of incidence (a) and microstructured targets irradiated at 45° (b–d) are presented as percentages of the total laser energy. The result of a laser pulse incident at 45° on a flat foil is indicated with dashed lines.

distribution, which can be seen from Figures 4c and 4d. Apart from increasing the absorption of laser energy by the plasma, the motion of the generated hot electrons will on average be more directed in the forward direction, thus decreasing the relative magnitude of the energy lost because of transverse transport of the hot electrons.

The effect of varying the incidence angle on the energy of forward and transverse motion of hot electrons, as defined by equations (1) and (2), is presented in Figure 5a. As expected the, the transverse motion energy

($\mathscr{E}_y$) steadily increases with the angle of incidence. The forward motion energy ($\mathscr{E}_x$) on the other hand first increases with the angle of incidence, peaks at 30° and then decreases. This is mainly due to the improved coupling between the electric field of the laser and the plasma across the surface for oblique incidence. Furthermore, it should be pointed out that the total energy of electrons transiting the virtual surface is slightly larger than the total absorbed laser energy, as seen in the figure, due to double counting of refluxing particles mainly associated with the local heating of the plasma by the main pulse.

Instead, looking at how these quantities are affected by microstructures of varying shape and size, we see that the transverse motion energy remains relatively unchanged as the linear scale of the structures increase. An interesting exception to this is the triangular structures, which instead displays a strong peak at a size of $d/\lambda = 1/2$. What is more important however, is the fact that the forward energy is greatly improved for $1/2 \lesssim d/\lambda \lesssim 2$ for all three cases. Thus, the additional energy transferred to the hot electrons is mainly contributing to their forward motion. As previous studies have not considered this separation it is difficult to make a straightforward comparison of the key results of this paper. However it can still be noted that, based on the total absorption also presented in Figure 5, our findings agree with previous studies of similar setups on, e.g., an optimal structure size of around $d/\lambda = 1/2$ and a total absorption of above 50% [42,43].

Since the relative energy of forward motion can be seen to increase with the addition of the microstructures, it is interesting to also compare the targets using this measure, as it provides information about the relative amount of energy of the electrons expected to be useful to applications such as TNSA, in which case "useful" is taken to mean: transferable to the ions at the rear surface. As can be seen from Figure 6 the relative energy of forward motion for the three structured designs follows a very similar trend, despite their differences in absolute energy, as seen in Figures 5b–5d. Furthermore the relative energy of forward motion displays a decreasing trend with increasing angle of incidence and with 0° being the optimal angle, in terms of electron directionality, as expected. However such angles, close to normal incidence, are generally avoided for technical reasons in order to minimize the risk of damaging the laser by back reflections. Moreover, Figure 6 seem to suggest that the near-normal incidence flat target performs better than the microstructured targets. However one should take into account that Figure 6 only shows that the hot electrons to a higher degree are forward directed, with a larger percentage of their energy residing in their forward motion, than for the microstructured targets and, from Figure 5, we still have that the absolute energy of the hot electrons is much larger with the structures than without.

Note that the momentum distribution of the hot electrons is widely different for the flat and structured targets, as demonstrated by Figure 4. The momentum distribution is centered about the line described by equation (6) for flat targets but is more centered around the target normal for the case of microstructured targets.

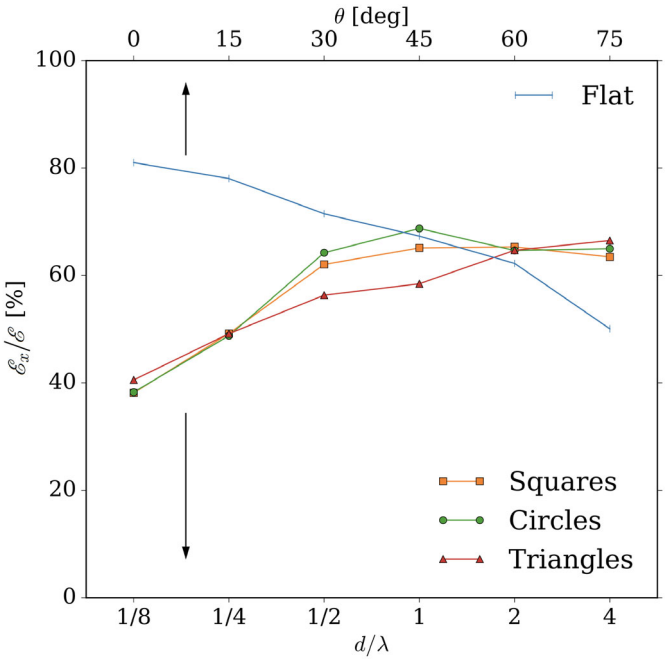

Fig. 6. The energy stored in forward motion of electrons transiting a virtual surface located 1 μm inside the plasma slab presented as percentage of the total kinetic energy of the transiting electrons. The upper x-axis represents the laser incidence angle for the flat target, while the lower x-axis represents the structure size of the microstructured targets, irradiated at an incidence angle of 45°.

Moreover, a clear discrepancy between the total absorption and total energy of the transiting hot electrons can be seen for mainly sub-wavelength square and circular structures, presented in Figures 5b and 5c. Taking into consideration that at least some double counting occurs in calculating the transit energy makes this difference all the more significant. This clearly shows that a significant portion of the absorbed energy does not get carried across the virtual surface, by the electrons. A fraction of this energy can be found in the semi-static fields forming at the plasma interface, but the lion's part can be found as kinetic energy of hot electrons trapped by a shock front, thus being prevented from travelling further into the plasma. It is also interesting to note that this behaviour is much less pronounced with the triangular structures which opens up for the possibility of controlling it by smart design choices.

4 Conclusions

In this paper we consider energy partitioning among transverse and longitudinal motion of accelerated electrons, under the influence of microstructures on the front side of the target. First, we analyses the limitations of the process in terms of laser energy absorption and spectral properties of the generated hot electrons. We found, expectedly, that the absorption indeed was affected by the microstructures, and that the size of the structures affected the absorption.

However, we also found that the hot electron distribution was significantly affected by the target structures.

We would like to stress the importance of the latter findings. As stated, it is well-known that front surface structures affects the general absorption properties of the target. But not only can the structures increase the total absorption, they can also alter the transverse transport of the hot electrons. This can enable a stronger acceleration of the ions of interest.

Our findings also points us to the following interesting conclusions:

- There is a limited view of the TNSA scheme when *only* considering increased absorption: it is only possible to obtain a few times stronger absorption by structuring the targets, as given in this paper, and it is only possible to further improve this by about a factor of 2 (being bounded by 100%), but for most applications we would require the energy transfer to go much further.
- The partitioning of energy in the hot electron distribution can be altered by about 20% by the use of microstructures. Thus, it may be important for TNSA in particular; only the electron momenta in the x-direction can be considered beneficial for ion acceleration, as large transverse momenta will represent an energy loss channel in this sense.
- However, a large angular divergence of electrons leads to small ion angular divergence, but also a small cutoff ion energy, and a smaller electron angular divergence leads to larger ion divergence, but also increased cutoff energy; thus, there is a trade-off.

As final conclusion, we find that it is of central importance to control the electron distribution. For this purpose, improvements can be made in the stages after the electron heating, using, e.g., strong guiding magnetic fields or mass limited targets. There is also the possibility of using targets cleverly designed to take advantage of the directionality of the hot electrons or to guide their transverse motion in order to increase the energy transferred from the electrons to the ions, see for example Burza et al. [25]. There are thus ample opportunities for future studies and improvements of the TNSA scheme.

The authors would like to thank the PICADOR development team, and S. Bastrakov in particular, for their invaluable technical support and acknowledge the financial support by the Wallenberg Foundation through the grant "Plasma based compact ion sources" (PLIONA). The simulations were performed on resources provided by the Swedish National Infrastructure for Computing (SNIC) at HPC2N.

Author contribution statement

All the authors were involved in the preparation of the manuscript. All the authors have read and approved the final manuscript.

References

1. U. Teubner, P. Gibbon, Rev. Mod. Phys. **81**, 445 (2009)
2. H. Daido et al., Rep. Prog. Phys. **75**, 056401 (2012)
3. A. Macchi et al., Rev. Mod. Phys. **85**, 751 (2013)
4. S.S. Bulanov et al., Med. Phys. **35**, 1770 (2008)
5. M. Roth et al., Phys. Rev. ST Accel. Beams **5**, 061301 (2002)
6. P. Mora, Phys. Rev. Lett. **90**, 185002 (2003)
7. T.E. Cowan et al., Phys. Rev. Lett. **92**, 204801 (2004)
8. M. Passoni et al., New J. Phys. **12**, 045012 (2010)
9. T. Ditmire et al., Nature **386**, 54 (1997)
10. V.F. Kovalev et al., Phys. Plasmas **14**, 103110 (2007)
11. V.F. Kovalev et al., Phys. Plasmas **14**, 053103 (2007)
12. T. Esirkepov et al., Phys. Rev. Lett. **89**, 175003 (2002)
13. T. Esirkepov et al., Phys. Rev. Lett. **96**, 105001 (2006)
14. S.S. Bulanov et al., Phys. Rev. E **78**, 026412 (2008)
15. L.O. Silva et al., Phys. Rev. Lett. **92**, 015002 (2004)
16. D. Haberberger et al., Nat. Phys. **8**, 95 (2012)
17. T. Schlegel et al., Phys. Plasmas **16**, 083103 (2009)
18. T. Esirkepov et al., Phys. Rev. Lett. **92**, 175003 (2004)
19. S.V. Bulanov et al., Phys. Rev. Lett. **104**, 135003 (2010)
20. A. Henig et al., Phys. Rev. Lett. **103**, 245003 (2009)
21. S. Kar et al., Phys. Rev. Lett. **109**, 185006 (2012)
22. F. Mackenroth et al., Phys. Rev. Lett. **117**, 104801 (2016)
23. K.A. Flippo et al., Phys. Plasmas **15**, 056709 (2008)
24. S. Buffechoux et al., Phys. Rev. Lett. **105**, 015005 (2010)
25. M. Burza et al., New J. Phys. **13**, 013030 (2011)
26. S.A. Gaillard et al., Phys. Plasmas **18**, 056710 (2011)
27. K. Markey et al., Phys. Rev. Lett. **105**, 195008 (2010)
28. S.M. Pfotenhauer et al., New J. Phys. **12**, 103009 (2010)
29. M. Dalui et al., Phys. Plasmas **24**, 010703 (2017)
30. V. Floquet et al., J. Appl. Phys. **114**, 083305 (2013)
31. S. Jiang et al., Phys. Rev. Lett. **116**, 085002 (2016)
32. A. Lübcke et al., Sci. Rep. **7**, 44030 (2017)
33. D. Margarone et al., Phys. Rev. ST Accel. Beams **18**, 071304 (2016)
34. M. Passoni et al., Phys. Rev. Accel. Beams **19**, 061301 (2016)
35. D.B. Zou et al., Sci. Rep. **7**, 42666 (2017)
36. Y. Nodera et al., Phys. Rev. E **78**, 046401 (2008)
37. L. Cao et al., Phys. Plasmas **17**, 043103 (2010)
38. Z. Zhao et al., Phys. Plasmas **17**, 123108 (2010)
39. O. Klimo et al., New J. Phys. **13**, 053028 (2011)
40. D. Margarone et al., Phys. Rev. Lett. **109**, 234801 (2012)
41. A. Andreev et al., Phys. Plasmas **18**, 103103 (2011)
42. M. Blanco et al., New J. Phys. **19**, 033004 (2017)
43. A. Andreev et al., Plasma Phys. Control. Fusion **58**, 014038 (2016)
44. C. Riconda et al., Phys. Plasmas **22**, 073103 (2015)
45. T. Ceccotti et al., Phys. Rev. Lett. **111**, 185001 (2013)
46. S. Bastrakov et al., J. Comput. Sci. **3**, 474 (2012)
47. I.A. Surmin, S.I. Bastrakov, E.S. Efimenko, A.A. Gonoskov, A.V. Korzhimanov, I.B. Meyerov, Comput. Phys. Common. **202**, 204 (2016)